Transition-state Complex of the Purine-specific Nucleoside Hydrolase of T. vivax: Enzyme Conformational Changes and Implications for Catalysis

ARTICLE *in* JOURNAL OF MOLECULAR BIOLOGY · JULY 2006

Impact Factor: 4.33 · DOI: 10.1016/j.jmb.2006.03.026 · Source: PubMed

3 AUTHORS:

Wim Versées
Vrije Universiteit Brussel
49 PUBLICATIONS **970** CITATIONS
SEE PROFILE

John N Barlow
GlaxoSmithKline plc.
15 PUBLICATIONS **315** CITATIONS
SEE PROFILE

Jan Steyaert
Vrije Universiteit Brussel
136 PUBLICATIONS **4,599** CITATIONS
SEE PROFILE

doi:10.1016/j.jmb.2006.03.026 *J. Mol. Biol.* (2006) **xx**, 1–16

JMB

Available online at www.sciencedirect.com

SCIENCE DIRECT®

ELSEVIER

Transition-state Complex of the Purine-specific Nucleoside Hydrolase of *T. vivax*: Enzyme Conformational Changes and Implications for Catalysis

W. Versées*, J. Barlow and J. Steyaert

Laboratorium voor Ultrastructuur, Vrije Universiteit Brussel and Department of Molecular and Cellular Interactions, Vlaams Instituut voor Biotechnologie Pleinlaan 2, B-1050 Brussel Belgium

**Corresponding authors*

Nucleoside hydrolases cleave the *N*-glycosidic bond of ribonucleosides. Crystal structures of the purine-specific nucleoside hydrolase from *Trypanosoma vivax* have previously been solved in complex with inhibitors or a substrate. All these structures show the dimeric *T. vivax* nucleoside hydrolase with an "open" active site with a highly flexible loop (loop 2) in its vicinity. Here, we present the crystal structures of the *T. vivax* nucleoside hydrolase with both soaked (*Tv*NH-ImmH(soak)) and co-crystallised (*Tv*NH-ImmH(co)) transition-state inhibitor immucillin H (ImmH or (1*S*)-1-(9-deazahypoxanthin-9-yl)-1,4-dideoxy-1,4-imino-D-ribitol) to 2.1 Å and 2.2 Å resolution, respectively. In the co-crystallised structure, loop 2 is ordered and folds over the active site, establishing previously unobserved enzyme–inhibitor interactions. As such this structure presents the first complete picture of a purine-specific NH active site, including leaving group interactions. In the closed active site, a water channel of highly ordered water molecules leads out from the N7 of the nucleoside toward bulk solvent, while Trp260 approaches the nucleobase in a tight parallel stacking interaction. Together with mutagenesis results, this structure rules out a mechanism of leaving group activation by general acid catalysis, as proposed for base-aspecific nucleoside hydrolases. Instead, the structure is consistent with the previously proposed mechanism of leaving group protonation in the *T. vivax* nucleoside hydrolase where aromatic stacking with Trp260 and an intramolecular O5′-H8C hydrogen bond increase the pK_a of the N7 sufficiently to allow protonation by solvent. A mechanism that couples loop closure to the positioning of active site residues is proposed based on a comparison of the soaked structure with the co-crystallized structure. Interestingly, the dimer interface area increases by 40% upon closure of loop 2, with loop 1 of one subunit interacting with loop 2 of the other subunit, suggesting a relationship between the dimeric form of the enzyme and its catalytic activity.

Keywords: nucleoside hydrolase; transition-state analogue; crystal structure; loop movement; leaving group activation

Abbreviations used: NH, nucleoside hydrolase; PNP, purine nucleoside phosphorylase; PRT, phosphoribosyl transferase; IAG-NH, inosine-adenosine-guanosine preferring nucleoside hydrolase; IU-NH, inosine-uridine preferring nucleoside hydrolase; CU-NH, cytidine-uridine preferring nucleoside hydrolase; *Tv*NH, nucleoside hydrolase from *Trypanosoma vivax*; *Tv*NH–ImmH(co), structure of *Tv*NH co-crystallized with ImmH; *Tv*NH–ImmH(soak), structure of *Tv*NH soaked with ImmH; ImmH, immucillin H or [(1*S*)-1-(9-deazahypoxanthin-9-yl)-1,4-dideoxy-1,4-imino-D-ribitol]; ImmA, immucillin A or [(1*S*)-1-(9-deazaadenin-9-yl)-1,4-dideoxy-1,4-imino-D-ribitol]; DADMe-Imm, 4′-deaza-1′-aza-2′-deoxy-1′-(9-methylene)-immucillin; PzImmH, 8-aza-immucillin H or [(1*S*)-1-(7-hydroxy-1*H*-pyrazolo[4,3-*d*]pyrimidin-3-yl)-1,4-dideoxy-1,4-imino-D-ribitol]; pAPIR, *p*-aminophenyliminiribitol.

E-mail address of the corresponding author:
wversees@vub.ac.be

0022-2836/$ - see front matter © 2006 Published by Elsevier Ltd.

Introduction

In many enzymatic processes the enzyme participates dynamically in the reaction, undergoing large conformational changes and loop movements during catalysis. The study of the relationship between protein motion and enzyme catalysis is therefore an area of active research.[1–3] Mobile active site loops are also a common feature of *N*-ribosyltransferases, that include purine nucleoside phosphorylases (PNPs),[4,5] phosphoribosyl transferases (PRTs)[6–8] and nucleoside hydrolases (NH).[9]

Nucleoside hydrolases comprise a superfamily of structurally related calcium-dependent enzymes that hydrolyse the *N*-glycosidic bond of β-ribonucleosides to release the free nucleic base and ribose (Figure 1).[10] They are found in prokaryotes and eukaryotes but are absent from mammals. The exact metabolic role of the NHs is established only in parasitic protozoa, including the *Trypanosoma* genus, where they are key enzymes in the purine salvage pathway that aims to scavenge purines from their environment.[11,12] Since parasitic protozoa rely on the purine salvage pathway for survival, the NHs represent potential targets for antibiotic development. Moreover, in analogy with the high molecular mass PNPs, the NHs could constitute promising candidates for tumour-directed enzyme–prodrug strategies in cancer therapy.[13,14]

On the basis of sequence alignments the nucleoside hydrolases have been clustered into three groups.[15] The enzymes belonging to group I contain a conserved histidine in their nucleobase-binding pocket, which is replaced by a tryptophan in group II proteins and another amino acid residue (often a cysteine) in group III proteins. The functional data obtained on these proteins suggests that group I proteins include pyrimidine-specific nucleoside hydrolases and non-specific enzymes that accept both purine and pyrimidine nucleosides. Group II comprises purine-specific nucleoside hydrolases. The NHs of the third group are yet uncharacterised, and seem to pertain to multicellular organisms such as insects.

Crystal structures have been solved from NHs belonging to groups I and II.[15–17] These structures show the enzymes as homotetramers (for group I proteins) or homodimers (for group II proteins) of a globular α/β subunit. Their active sites contain a Ca^{2+} and are located at the C-terminal end of the central β-sheet. Only one inhibitor-complex structure has been solved for a group I NH, that of the non-specific NH (IU preferring NH or IU-NH) from the protozoon *Crithidia fasciculata* with the inhibitor *p*-aminophenyliminiribitol (pAPIR).[9] For group II NHs, a crystal structure has been solved of the purine-specific NH (IAG-preferring NH or IAG-NH) from *Trypanosoma vivax* in complex with a ground state inhibitor, 3-deaza-adenosine.[17] The structure of a slow mutant of this enzyme was also solved in complex with the genuine substrate inosine.[18]

Comparisons of unliganded and complexed NH structures from both groups I and II reveal substantial conformational changes. In the unliganded structures of both group I and II NHs, two

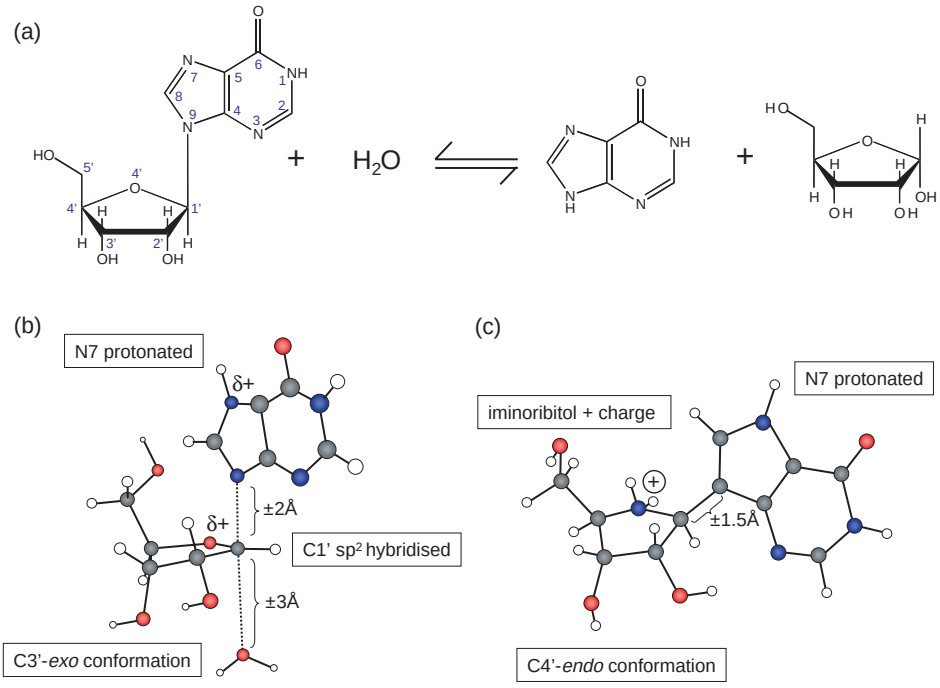

Figure 1. (a) The nucleoside hydrolase-catalysed hydrolysis reaction of a ribonucleoside (exemplified by inosine). The IUPAC–IUB atom numbering scheme is indicated in blue. (b) Proposed oxocarbenium-ion-like transition-state for the catalysed reaction. (c) The transition-state analogue inhibitor immucillin H (ImmH). The major structural and chemical features of the transition-state and inhibitor are indicated.

flexible loops (called loops 1 and 2) with low or no associated electron density are present on either side of the active site. Loop 1 is located at the C-terminal end of β3 and comprises residues 75–85; loop 2 is situated at the C-terminal end of a long α-helix and comprises residues 244–258 (*T. vivax* NH numbering, residues 220–239 in *C. fasciculata* NH). Upon binding of the inhibitor pAPIR on the group I IU-NH from *C. fasciculata*, loop 1 becomes ordered and loop 2 undergoes large conformational changes bringing several residues in the active site.[9] Unfortunately, information about the interactions between the leaving group pocket and the natural substrates is lacking due to the significant structural differences between the inhibitor and the natural purine/pyrimidine substrates. Binding of the ground state inhibitor 3-deaza-adenosine to the group II IAG-NH from *T. vivax* or of the substrate inosine to a slow mutant of this enzyme also orders loop 1. This brings Trp83 into a parallel stacking interaction with the nucleobase.[17,18] However, loop 2 remains totally unstructured in all group II structures thus far. Hence, a full view of the active site, that shows all the enzyme-substrate interactions, is still missing for any NH.

Kinetic isotope effects have shown that nearly all *N*-ribosyltransferases stabilize a transition-state with oxocarbenium ion character, with a nucleophilic displacement reaction mechanism varying from fully dissociative for nucleic acid processing enzymes to more moderately dissociative in the case of PNPs and NHs.[19] The transition-state of the latter enzymes shows a protonated purine base and little participation from the nucleophile.[20] Based on this transition-state structure, immucillin H (ImmH) (Figure 1) was developed as a picomolar inhibitor against human or bovine PNP.[21,22] It has also been reported to be a tight binding inhibitor of the IAG-NH of *T. brucei brucei* (K_I = 24 nM) and the IU-NH of *C. fasciculata* (K_I = 42 nM).[23] Its 4′-imino group replaces the O4′ ribosyl oxygen of inosine and, on protonation (pK_a = 6.9), mimics the partial positive charge of the ribooxocarbenium ion transition-state. The C–C glycosidic bond provides chemical stability. The deazahypoxanthine ring of ImmH is protonated at N7 (pK_a > 10) similar to inosine at the transition state. Subsequently, the DADMe immucillins were designed as closer mimics of highly dissociative *N*-ribosyltransferase transition states[24]: the position of the cation charge (pK_a N1′ ~ 9.2) is shifted to the position of the carbocation that is known to develop at the transition state, and the distance between the glycone and aglycone is increased *via* a methylene bridge.[25]

Here, we report the crystal structures of the *T. vivax* IAG-NH (*Tv*NH) either soaked or co-crystallised with the transition-state analogue inhibitor ImmH. The structure of *Tv*NH co-crystallised with ImmH represents the first image of a "closed" purine-specific nucleoside hydrolase with all loops entirely ordered and offers a complete picture of the interactions occurring in the transition state of the enzyme-catalysed reaction. The structures provide further insights in the mechanism of leaving group activation, the relation between enzyme activity and its multimeric state and suggest a possible mechanism leading to loop closure.

Results

Inhibition of *Tv*NH by immucillins

A selection of immucillins and DADMe-immucillins was screened in order to identify tight-binding inhibitors of *Tv*NH. Three immucillins, ImmH, ImmA and 8-aza-ImmH (or PzImmH),[26] displayed low nanomolar inhibition constants (Table 1). For the tightest binder, PzImmH, the K_d is a factor of 2000 lower than the K_M values reported for inosine and adenosine,[17] corresponding to an increase in binding energy of about 4 kcal/mol for the inhibitor compared to the natural substrates (in the simplified case where $K_M = K_S$). The weak inhibition shown by the DADMe-immucillins presumably results from the absence of the 2′-OH from these inhibitors, since 2′-deoxy-ribonucleosides are poor substrates for *Tv*NH.[18]

Of the three nanomolar inhibitors, only PzImmH displayed slow-onset inhibition, although all three inhibitors displayed slow-offset inhibition. Immucillins often display slow-onset inhibition as a result of a slow N4′ protonation step that follows the rapid equilibrium binding

Table 1. Inhibition constants for the interaction of immucillins and DADMe-immucillins with various nucleoside hydrolases

	IAG-NH *T. vivax* K_I (nM)			
	WT	R252A	IAG-NH *T. b. brucei* K_I (nM)[a]	IU-NH *C. fasciculata* K_I (nM)[a]
ImmH	6.2 ± 0.7	50 ± 7	24	42
ImmA	6.2 ± 0.3	13 ± 1	0.9[b]	7
PzImmH	1.2 ± 0.3[b]	ND[c]	1600	13900
DADMe-ImmH	> 1000	ND	ND	ND
DADMe-ImmA	> 100	ND	ND	ND
DADMe-ImmT	> 1000	ND	ND	ND

[a] Data taken from Evans *et al.*[26] and Miles *et al.*[23]
[b] Compound causes slow-onset tight binding inhibition characterised by K_I^*.
[c] Not determined.

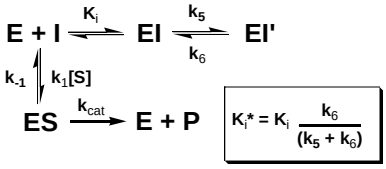

Scheme 1. Slow-onset inhibition for tight-binding inhibitors.[52]

step (Scheme 1).[27] For PzImmH, this allowed the microscopic rate constants associated with the EI⇔EI′ isomerisation step (Scheme 1) to be determined: $k_5 = 2.7 \times 10^{-3}\ s^{-1}$, $k_6 = 2.8 \times 10^{-4}\ s^{-1}$. The kinetics of the slow offset process for PzImmH were also sufficiently slow to allow active-site titration to be carried out. This indicated a monomer:inhibitor binding stoichiometry of 1:1, in contrast to the half-the-sites activity previously reported for substrate turnover.[28] Table 1 also compares the obtained K_I values to the corresponding values for other NHs.[26] While the binding properties of ImmH and ImmA are comparable between the different NHs, PzImmH shows significantly tighter binding to the IAG-NH from *T. vivax*. This is intriguing because the IAG-NH from *T. vivax* and *T. brucei brucei* show high sequence identity in the region of the active site postulated to be involved in purine aglycone binding.

Global fold of *Tv*NH–ImmH complexes

Two different crystal structures of the wild-type *T. vivax* NH in complex with ImmH were solved (see Table 2 for refinement statistics). The first complex was obtained by soaking the inhibitor in a pre-existing protein crystal (*Tv*NH–ImmH(soak)). This structure was refined to 2.1 Å resolution, yielding a final *R*-factor of 17.81% (R_{free} = 22.52%). Since conformational changes induced by inhibitor binding can be potentially obstructed by crystal packing restraints when soaking an inhibitor into a crystal, a second complex was generated by co-crystallisation of ImmH with the enzyme (*Tv*NH–ImmH(co)). This structure was refined to 2.2 Å resolution, yielding a final *R*-factor of 16.74% (R_{free} = 22.61%).

Both complexes contain a homodimer in the asymmetric unit with both active sites fully occupied with ImmH. All monomers show the characteristic α/β core composed of an eight-stranded mixed β-sheet, with seven parallel and one antiparallel strand, and several surrounding α-helices.[10,16,17] The *Tv*NH–ImmH(soak) complex shows an open protein structure (Figure 2). Loop 1 (amino acid residues 75–85) that consists of a coil connecting β3 to α3 and the N-terminal part of α3, was included in the model but shows great flexibility, typified by high *B*-factors. Main-chain *B*-factors in this region are as high as 65 Å^2, compared to a mean *B*-factor of 29 Å^2 for all main-chain atoms. Loop 2 is completely disordered and the corresponding residues (residues 245–257 in subunit A and 245–255 in subunit B) were omitted from the model due to a lack of electron density. Both ImmH molecules are also loosely bound in the active site, with a mean *B*-factor of 50 Å^2 calculated over all atoms of both ImmH molecules. No significant conformational changes could be observed upon comparing the *Tv*NH-ImmH(soak) complex with the unliganded *Tv*NH (PDB 1HOZ).

By contrast, the co-crystallised complex *Tv*NH–ImmH(co) shows a closed conformation, with significant conformational changes in the loops

Table 2. Data collection and refinement statistics

	*Tv*NH–ImmH(soak)	*Tv*NH–ImmH(co)
Diffraction data		
Space group	$P2_1$	$P2_1$
a (Å)	51.50	54.19
b (Å)	73.11	74.39
c (Å)	82.35	73.96
β (deg.)	104.10	98.38
Resolution range (Å)[a]	25.0–2.0 (2.07–2.00)	50.0–2.2 (2.28–2.20)
R_{sym} (%)[a]	5.9 (34.1)	21.8 (37.1)
$I/\sigma I$[a]	13.27 (3.85)	9.12 (4.08)
Completeness (%)[a]	99.9 (99.9)	100 (100)
Structure refinement		
Resolution range (Å)	25.0–2.07	50–2.2
R_{cryst} (%)	17.81	16.74
R_{free} (%)	22.52	22.61
rmsd for bond lengths (Å)	0.0097	0.0079
rmsd for bond angles (deg.)	1.554	1.439
Ramachandran plot (% most favoured, allowed, generously allowed, disallowed residues)	90.0, 9.5, 0.4, 0.2	88.7, 11.3, 0, 0
No. atoms per a.u.	5263	5490
Average *B*-factors (Å^2) (protein, water, ImmH)	30.49, 39.93, 50.06	19.78, 28.01, 15.05

$R_{sym} = \Sigma|I_i(hkl) - \langle I_i(hkl)\rangle| / \Sigma I_i(hkl)$, where I_i (hkl) are the intensities of multiple measurements and $\langle I_i\ (hkl)\rangle$ is the average of the measured intensities for the *i*th reflection. $R_{cryst} = 100 \times \left(\sum_h |F_{obs,h} - F_{calc,h}| / \sum_h F_{obs,h}\right)$, where F_{obs} and F_{calc} are observed and calculated structure amplitudes, respectively. $R_{free} = R_{cryst}$ calculated for the test set of reflections not used in refinement.

[a] Values in parentheses are for the highest resolution shell.

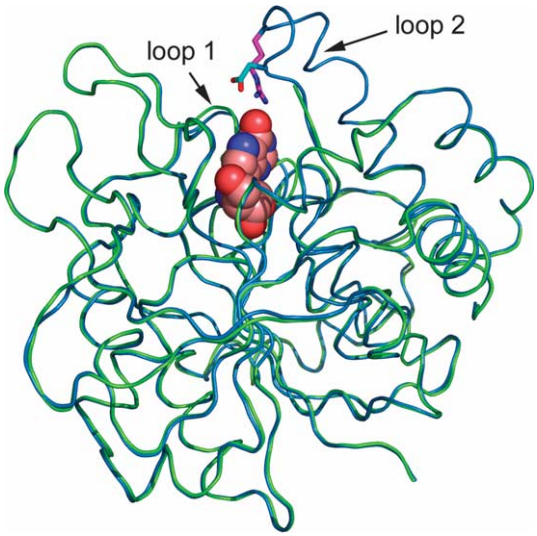

Figure 2. Superposition of a subunit of *Tv*NH–ImmH(soak) (shown in green) and *Tv*NH–ImmH(co) (shown in blue). ImmH is shown in a CPK representation. Loop 1 and loop 2 are indicated by arrows. Loop 2 is visible only in the *Tv*NH–ImmH(co) structure. Residues Arg252 (purple) and Asp255 (cyan) on loop 2 are shown as sticks. The Figure was made with PyMOL.[60]

surrounding the active site being evident (Figure 2). Loop 1 is completely fixed with *B*-factors as low as the mean value for the entire protein. Loop 2 closes over the active site and clear density is present for the entire loop (although *B*-factors are somewhat higher than the mean). The N-terminal part of loop 2 (amino acid residues 245 to 252) adopts a helical secondary structure and forms a kinked C-terminal extension to helix α10 (see Versées *et al.*[17] for numbering of the helices). The C-terminal part of loop 2 forms a coil connecting α10 to α11. The ordering of loop 2 brings residues Arg252, Asp255 and Tyr257 into the active site. The side-chain of Arg252 extends entirely into the active site and interacts with the O6 exocyclic carbonyl of ImmH. The closing of the *Tv*NH–ImmH(co) structure also results in an increased ordering of the ImmH ligand in the active site with a mean *B*-factor of 15 Å^2, lower than the mean *B*-factor over all protein main-chain atoms (19 Å^2). The rest of the protein backbone is mainly unaffected by ImmH binding, with an rms deviation of 0.299 Å between all main-chain atoms of one subunit of *Tv*NH-ImmH(co) and of the unliganded *Tv*NH (PDB 1HOZ), and besides the two loops no other large conformational changes are observed. Furthermore, no significant asymmetry is observed in the global fold of the A and B subunits of the *Tv*NH-ImmH(co) structure, with an rms deviation of 0.318 Å between all main-chain atoms of both subunits.

Quaternary structure

In contrast to all group I nucleoside hydrolases (IU-NH and CU-NH), which are tetramers,[9,15] the IAG-NH from *T. vivax* is a dimer in the crystal structure.[29] The dimer interface of the latter differs completely in comparison to the subunit interfaces in the group I NHs, involving different secondary structure elements. In *Tv*NH the dimer interface is formed by the helices α3, α9 and α10, with α3 of one monomer interacting with α9 and α10 of the other subunit. The accessible surface area (ASA) buried in the interface of the unliganded *Tv*NH (PDB 1HOZ) is about 876 Å^2 and is mainly non-polar. In the complexes with 3-deaza-adenosine (PDB 1HP0) and inosine (PDB 1KIC) the interfacial ASA is increased to 1043 Å^2 and 920 Å^2, respectively, primarily as a result of loop 1 ordering. In the *Tv*NH–ImmH(soak) complex, the buried ASA (867 Å^2) is similar to the unliganded *Tv*NH, stressing again the open nature of this complex. However, ordering of loop 1 and loop 2 in the *Tv*NH-ImmH(co) complex results in an increase of the buried ASA to 1232 Å^2, significantly higher than in either the unliganded or 3-deaza-adenosine/inosine bound forms. Part of this increase results from a lengthening of helices α3 and α10 (*via* ordering of loop 1 and loop 2, respectively), that form part of the dimer interface (Figure 3). Furthermore, the ordered loop 1 (α3) of one subunit interacts with the ordered loop 2 (α10) of the other subunit and *vice versa*. Several new contacts (including one hydrogen bond) are formed between residues of α3 of one subunit and α10 of the other subunit. The α-helical part of loop 2 also interacts with the loop connecting β2 with α2 of the other subunit. This latter loop harbours the active site residue Asp40. These new interface interactions cause a small rotation (about 3°, with the rotation axis nearly perpendicular to the α10 helices) of one subunit with respect to the other compared to the unliganded *Tv*NH, bringing the active sites slightly closer to each other.

ImmH properties

Table 3 lists the parameters describing the conformation of ImmH bound to the active site of *Tv*NH and compares these with other ligands bound in the active site of NHs. The iminoribitol moiety adopts a C4′-*endo* conformation, corresponding to a pseudorotation phase angle of about 230°. This conformation differs from the preferred C2′-*endo* conformation of free ImmH[4] and is energetically unfavourable.[29] However, in substrates this conformation favours the formation of a ribooxocarbenium-ion transition state due to an N9–C1′–C2′–H2′ dihedral angle of 0°, allowing orbital overlap between the breaking N9–C1′ bond and the C2′–H2′ bond.[20] A comparable conformation was observed for ImmH bound to calf spleen PNP.[4] Also inosine bound in the active site of the slow Asp10Ala mutant of *Tv*NH adopts a similar conformation.[18] The 5′OH torsion angle (O5′–C5′–C4′–N4′) ranges from 39° to 50° and is on average somewhat lower than the

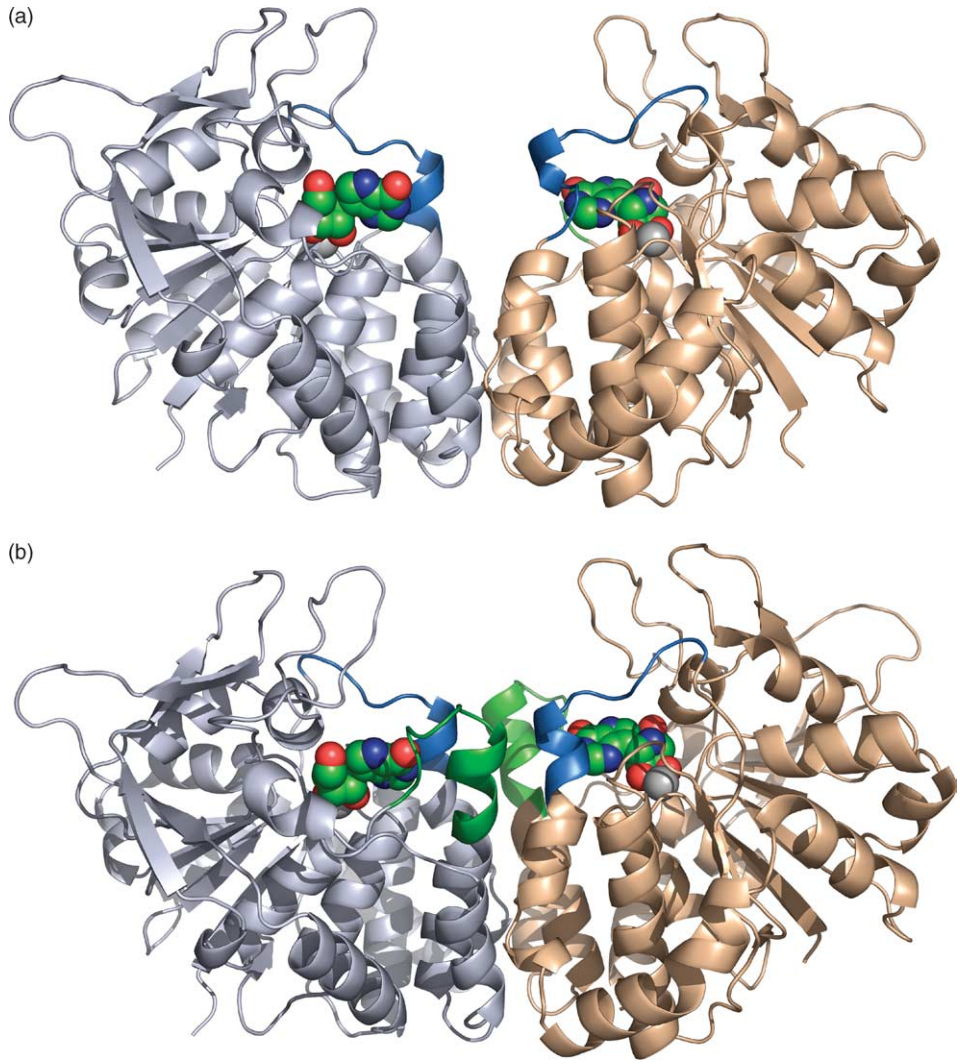

Figure 3. Comparison of the quaternary structure and subunit interface of *Tv*NH–ImmH(soak) (a) and *Tv*NH–ImmH(co) (b). Loop 1 is shown in blue, loop 2 in green. The Ca^{2+} is shown as a grey sphere, ImmH is represented as a CPK model. The Figure was made with PyMOL.[60]

corresponding angle observed in the *Tv*NH(Asp10Ala)–inosine complex, bringing the 5′OH closer above the ribosyl ring. The glycosidic torsion angle χ (N4′–C1′–C9–C4) is close to 180°, characteristic of an *anti* conformation with the base pointing away from the ribose moiety. The same orientation was observed for inosine bound to *Tv*NH(Asp10Ala), while a *syn* conformation was observed for 3-deaza-adenosine bound to the wild-type *Tv*NH.[17] A recent molecular dynamics study suggested the *syn* conformation as catalytically relevant.[30] This simulation suggested that the ground state substrate could bind in either *syn* or *anti* conformation, but that during the reaction the substrate in the *anti* conformation underwent base flipping. Our present study disfavours this hypothesis, since it shows the transition-state analogue tightly bound in the *anti* conformation, suggesting the latter conformation as the catalytically relevant one.

Active site: *Tv*NH–ImmH interactions

Four ImmH–protein interactions newly appear or are changed by more than 0.3 Å† in the *Tv*NH–ImmH(co) structure compared to the previous *Tv*NH complexes (see Table 4 and Figure 4). A first striking difference is the interaction between Arg252 and the O6 carbonyl of the 9-deazahypoxanthine ring of ImmH. The side-chain of Arg252 is brought into the active site by the closure of loop 2, placing its NH2 atom within 2.4 Å (2.5 Å in the A subunit) of O6. The Arg252 side-chain is further held in place by an interaction of its other guanido N-atom with the carboxyl side-chain and carbonyl main-chain of Asp255, also a residue of loop 2.

† A 0.3 Å cut-off was applied for significance of interaction distance differences on the basis of a Luzzati coordinate error of 0.21 Å for *Tv*NH–ImmH(co).[62,63]

Table 3. Conformation of ligands in the active sites of various NH-complexes: immH co-crystallized with *Tv*NH (both subunits); immH soaked in the active site of *Tv*NH (both subunits); inosine in complex with D10A mutant of *Tv*NH (taken from PDB 1KIC); 3-deaza-adenosine in complex with *Tv*NH (taken from PDB 1HP0) and pAPIR in complex with *Cf*NH (taken from PDB 2MAS)

	χ[a] (deg.)	P[b] (deg.)	ϕ_{oo}[c] (deg.)	Ribose conf.
*Tv*NH–immH(co) A	−169 (*anti*)	229	48	C4′-*endo*
*Tv*NH–immH(co) B	−169 (*anti*)	230	39	C4′-*endo*
*Tv*NH–immH(soak) A	−173 (*anti*)	232	50	C4′-*endo*
*Tv*NH–immH(soak) B	−165 (*anti*)	233	46	C4′-*endo*
*Tv*NH D10A-ino	−176 (*anti*)	236	58	C4′-*endo*
*Tv*NH-3-deaza-ado	−1 (*syn*)	100	70	O4′-*endo*
*Cf*NH–pAPIR	ND	233	24	C4′-*endo*

[a] Torsion angle O4′(or N4′)–C1′-N9(or C9)–C4.
[b] Pseudorotation phase angle, calculated as described.[29]
[c] Torsion angle O5′–C5′–C4′–O4′(or N4′).

A second interaction with the leaving group not detected in the other structures is the interaction between Asp40 and the N3 atom of ImmH, with the carboxyl oxygen of Asp40 located at 2.6 Å from the N3. In all the previous structures, this interaction was not observed because of experimental artefacts. In the *Tv*NH–3deaza-adenosine complex this interaction was impossible because of the *syn* conformation of the leaving base vis-à-vis the ribose. In the Asp10Ala mutant, Asp40 was shifted away from the base due to the mutation. The pK_a of Asp40 in a docked enzyme–substrate complex was recently calculated to be approximately 7.2 to 7.8, making it protonated at physiological pH and allowing a hydrogen bond with N3.[30]

A third difference in the leaving group pocket concerns the indole side-chain of Trp260, which moves closer to the 9-deazahypoxanthine ring. Trp260 is involved in a tilted parallel aromatic stacking interaction with the leaving group, and in the transition-state complex the CH2 atom of Trp260 moves 0.6 Å closer to the N7 of ImmH.

In contrast to the ribose moiety of substrates, ImmH is likely to be protonated (at N4′) in the *Tv*NH–ImmH(co) structure,[31] introducing a full positive charge where none was present in the other crystal complexes. Despite this extra charge, little change is apparent in the binding interactions in this region of the active site, the only difference being a closer interaction of Asn186 with the

Table 4. List of interaction distances (given in Å) in the active sites of *Tv*NH–ImmH(co), *Tv*NH–ImmH(soak), *Tv*NH Asp10Ala-inosine (PDB 1KIC) and *Tv*NH-3-deaza-adenosine (PDB 1HP0)

	*Tv*NH–ImmH(co)	*Tv*NH–ImmH(soak)	*Tv*NH(D10A)–inosine	*Tv*NH–3-deaza-ado
Enzyme–ribose				
Asp14(OD1)–O2′	2.73	2.70	2.55	2.68
Asp261(OD1)–O3′	2.52	2.47	2.67	2.58
Asn186(ND2)–O3′	3.14	3.09	3.04	2.95
Asn186(OD1)–O4′/N4′	**3.05**	**3.24**	**3.88**	**4.11**
Asn173(ND2)–O5′	2.69	2.66	2.94	3.00
Glu184(OE1)–O5′	2.74	2.65	2.57	2.64
Ca^{2+}–O2′	2.44	2.46	2.51	2.39
Ca^{2+}–O3′	2.33	2.59	2.49	2.42
Wat2 (nucleophile)–C1′	3.27	3.22	ND[a]	3.34
Enzyme–nucleobase				
Trp260(CH2)–N7	**3.18**	**3.50**	**3.79**	**ND**[a]
Trp83(CZ3) – N7	3.46	3.49	ND[a]	ND[a]
Asp40 (OD2)–N3	**2.58**	**2.65**	**ND**[a]	**ND**[a]
Arg252 (NH2)–O6	**2.37**	**ND**[a]	**ND**[a]	**ND**[a]
Wat4–N7	2.62	2.75	2.65	ND[a]
Intra-substrate				
O5′–C8	3.06	3.20	3.32	ND[a]
O5′–O4′/N4′	2.83	2.87	2.83	2.71
Intra-enzyme				
Asp10–Wat2 (nucleophile)	2.57	2.65	ND[a]	2.58
Wat4–Wat215	2.58	ND[a]	ND[a]	ND[a]
Wat4–Wat217	2.76	ND[a]	ND[a]	ND[a]
Arg252 (NH1)–Wat4	3.23	ND[a]	ND[a]	ND[a]
Asp255(OD1)–Wat215	2.96	ND[a]	ND[a]	ND[a]
Asp255(OD2)–Wat217	2.56	ND[a]	ND[a]	ND[a]
Gly256 (O)–Wat215	2.68	ND[a]	ND[a]	ND[a]
Asn173 (O)–Wat217	2.91	ND[a]	ND[a]	ND[a]

Distances were taken from the B subunit of each complex.
[a] Not applicable or changed due to mutation.

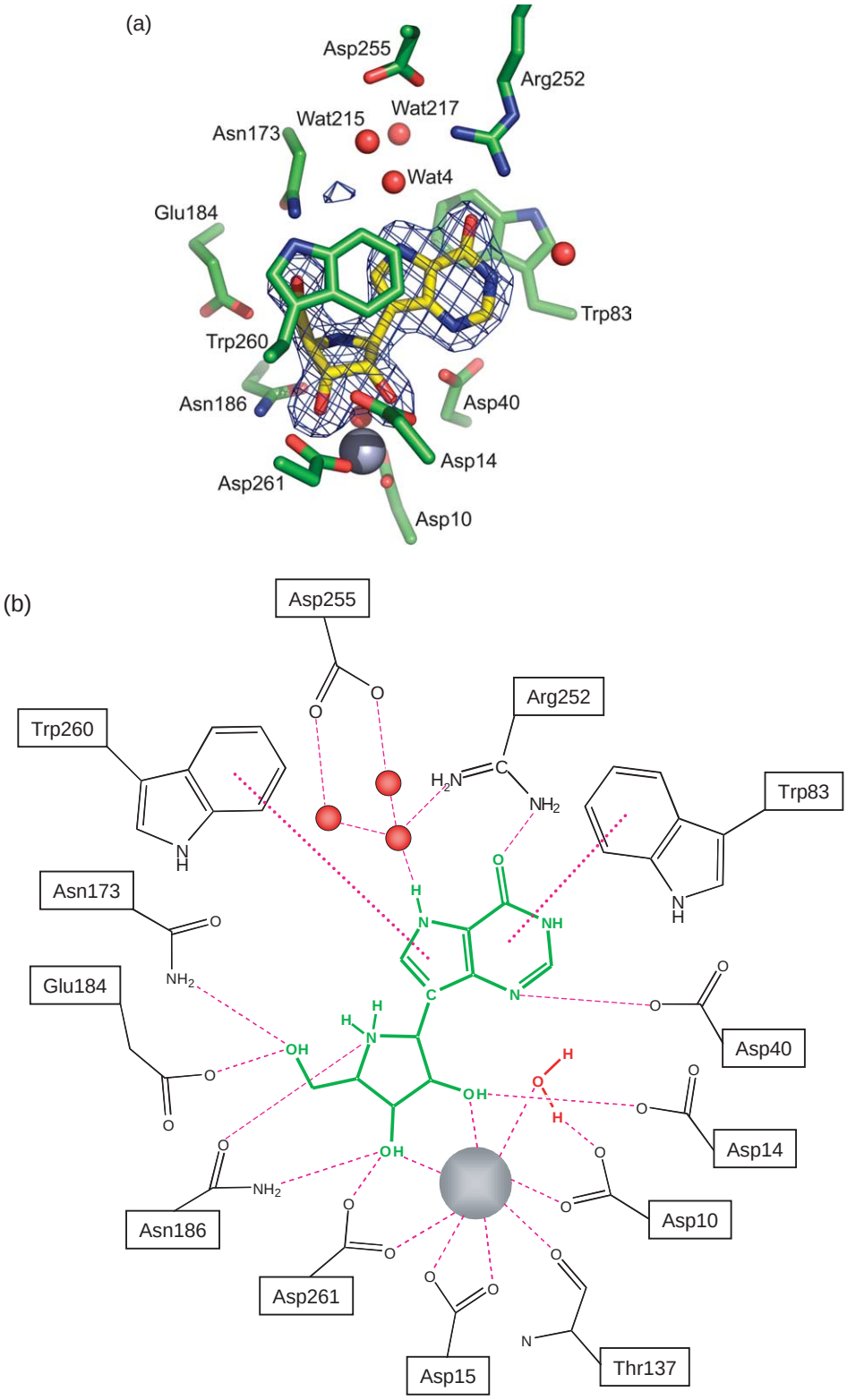

Figure 4. (a) Active site of the closed *Tv*NH–ImmH(co) structure. The residues Arg252 and Asp255 are provided by loop 2. The bound inhibitor, ImmH, is shown in yellow. The electron density, contoured at 3σ, of an $F_o - F_c$ simulated annealed omit map calculated without the inhibitor is also shown. The Ca^{2+} and water molecules are represented as grey and red spheres, respectively. The "nucleophilic" water molecule, three water molecules forming a water channel from the N7 of the nucleobase toward bulk solvent, and a water molecule interacting with the N1 of the nucleobase are shown. The numbering of the B-subunit is used for the water molecules. The Figure was made with PyMOL.[60] (b) Schematic representation of interactions in the active site of the *Tv*NH-ImmH(co) structure. ImmH is shown in green. The color codes for the Ca^{2+} and water molecules are the same as above.

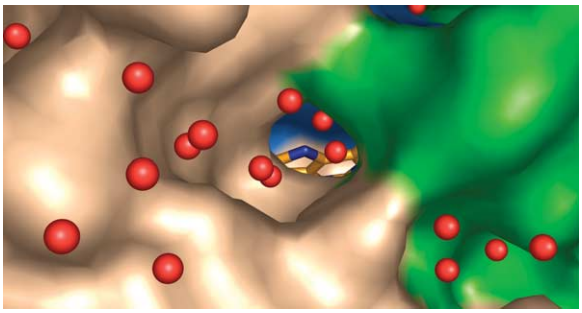

Figure 5. Molecular surface of *Tv*NH–ImmH(co) around the active site, calculated without ImmH. ImmH is shown in the active site, with its carbon atoms coloured gold. A channel of water molecules (depicted as red spheres) leading from the N7 of ImmH toward bulk solvent is apparent. Residues from loop 1 are coloured blue, residues from loop 2 are coloured green. The Figure was made with PyMOL.[60]

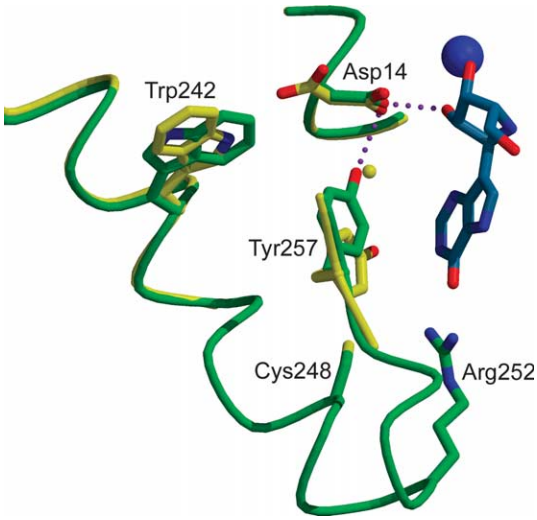

Figure 6. Proposed mechanism for loop 2 closure. A superposition of the relevant residues of *Tv*NH–ImmH(co) and *Tv*NH–ImmH(soak) is shown. *Tv*NH–ImmH(co) with a closed loop 2 is coloured green, *Tv*NH–ImmH(soak) with an unstructured loop 2 is coloured yellow. The inhibitor (in grey) and the Ca^{2+} (blue sphere) are also shown. Flipping of the Trp242 side-chain in *Tv*NH–ImmH(co) compared to *Tv*NH–ImmH(soak) forces Asp14 into a "catalytic" conformation. This conformation allows Asp14 and Tyr257 to interact, pulling Tyr257 into the active site with concomitant release of a bridging water molecule (shown as a yellow sphere). The void left by Tyr257 is then occupied by residues from loop 2, allowing the structuring of this loop (see the text for further details). The Figure was made with MOLSCRIPT.[61]

inhibitor. The Asn186 side-chain carbonyl is located at 3.05 Å from the N4′, while the corresponding distance with the O4′ in the Asp10Ala–inosine complex was almost 3.9 Å.

The N7 and N1 of the leaving group in the *Tv*NH–ImmH(co) complex do not interact with any enzyme residues. Instead, both nitrogen atoms interact with bulk water *via* a channel of highly ordered water molecules (Figures 4 and 5). This is especially apparent in the case of N7. Using the numbering of the B subunit, N7 is hydrogen bonded to wat4 (N–O distance of 2.66 Å). This water in its turn is hydrogen bonded to two other water molecules, wat215 and wat217, and so forth. These water molecules are tightly held in place *via* numerous interactions with amino acid residues, mainly provided by loop 2. *B*-factors for wat4, wat215 and wat217 are 22.6 $Å^2$, 19.9 $Å^2$ and 19.8 $Å^2$, respectively, compared to a mean of 19.0 $Å^2$ for all protein atoms (this is even more pronounced for the corresponding water molecules in the A subunit with *B*-factors of 15.7 $Å^2$, 9.2 $Å^2$ and 17.8 $Å^2$, respectively). wat4 interacts with the side-chain of Arg252; wat215 is within interaction distance with the side-chain of Asp255 and the main-chain carbonyl of Gly256; and wat217 is within interaction distance with the side-chain of Asp255 and the main-chain carbonyl of Asn173.

Mechanism of loop closure

A possible route leading to the closure of loop 2 upon ImmH binding (Figure 6) is suggested by the observed "flipping" of the Trp242 side-chain in the *Tv*NH–ImmH(co) structure, as compared to all other *Tv*NH crystal structures solved so far (the Trp242 dihedral angle CA–CB–CG–CD2 is 3.2° and 189° in *Tv*NH–ImmH(co) and *Tv*NH–ImmH(soak), respectively). Trp242 is part of helix α10 at the N-terminal side of loop 2. In most previously solved structures, Asp14 adopted two alternative conformations: one "catalytic conformation" pointing toward the 2′OH, and another "non-catalytic conformation" pointing away from the active site. In the *Tv*NH–ImmH(co) structure Asp14 is prevented from assuming the non-catalytic conformation by the side-chain of Trp242†. The locked catalytic conformation of Asp14 allows it to form a new interaction with the phenol OH of Tyr257 (3.27 Å), which is located at the C terminus of loop 2. In *Tv*NH–ImmH(co) the Tyr257 side-chain rotates compared to its position in the *Tv*NH–ImmH(soak) complex, placing its hydroxyl group deeper into the active site. In the *Tv*NH–ImmH(soak) complex the side-chains of Tyr257 and Asp14 hydrogen bond to the same bridging water molecule, which is released upon loop closure. Loop closure also results in closer interactions of the Tyr257 with the side-chain of Asn12 (2.76 Å *versus* 3.26 Å) and the main-chain amide nitrogen from Asp14 (3.11 Å *versus* 6.27 Å)(not shown in Figure 6). The void left by the dislocation of the Tyr257 side-chain is

† Note that the alternative order of events, where ImmH forces Asp14 into the catalytic conformation, allowing the Trp242 side-chain to flip, is also possible.

Table 5. Comparison of steady-state kinetic parameters of Arg252Ala and Asp40Ala mutants with the wild-type *Tv*NH

	Arg252Ala		Asp40Ala		Wild-type[a]	
	k_{cat} (s^{-1})	K_M (μM)	k_{cat} (s^{-1})	K_M (μM)	k_{cat} (s^{-1})	K_M (μM)
Guanosine	9.8±0.5	31±5	2.7±0.2	66±8	2.3±0.1	2.3±0.5
7-Methyl-guanosine	13.2±0.6	2.4±0.6	13.6±0.8	8±2	3.4±0.1	2.1±0.3
Adenosine	5.7±0.2	6.6±0.7	ND[b]	ND[b]	2.6±0.2	8±2
Purine riboside	2.0±0.1	11±1	ND[b]	ND[b]	3.9±0.1	4±1
Cytidine	0.54±0.06	1060±300	ND[b]	ND[b]	0.338±0.005	925±39

k_{cat} is calculated per active site. All measurements were performed at 35 °C in 20 mM Hepes (pH 7.0), 150 mM NaCl, 1 mM $CaCl_2$.
[a] Data taken from Versées *et al.*[18]
[b] Not determined.

filled by residues Cys248 and Arg252 of loop 2, allowing loop 2 to adopt its closed conformation.

Role of Asp40 and Arg252 in the catalytic mechanism

The closed active site of *Tv*NH–ImmH(co) shows two new possible enzyme-leaving group interactions involving Arg252 and Asp40. To probe the contribution of these residues to catalysis, both were mutated to alanine and the effect of these mutations on the hydrolysis rate of various substrates was monitored using steady-state kinetics (Table 5). The fraction of this catalytic contribution owing to leaving group activation can be quantified by comparing the hydrolysis rate of guanosine with that of 7-methylguanosine. The latter is a substrate analogue with an activated (positively charged) purine ring, needing no further leaving group activation.[32,33]

The Arg252 guanido-group (located on loop 2) is situated at about 2.5 Å from the exocyclic carbonyl at position 6 of ImmH, suggesting a strong interaction. However, mutation of Arg252 to alanine resulted in only small changes in k_{cat}/K_M and k_{cat} for the substrates tested†. Thus, Arg252 appears to play a minor role in catalysis, consistent with the observation that wild-type *Tv*NH displays similar k_{cat}/K_M values and k_{cat} values for guanosine (carbonyl group at position 6), adenosine (amino group at position 6) and purine riboside (no exocyclic group at position 6).[18] Moreover, Arg252 does not seem to contribute to the discrimination shown by *Tv*NH against pyrimidine nucleosides, since mutating it has no effect on the kinetics of cytidine hydrolysis. Mutation of Arg252 does have a small effect on binding, as reflected by the ca fivefold increase in K_M for Guo and K_I for ImmH, while the K_M for adenosine and K_I for ImmA remain relatively constant (Table 1).

A larger effect was seen upon mutation of Asp40 to alanine, which resulted in a 25-fold decrease in k_{cat}/K_M for guanosine but, interestingly, no change in k_{cat}/K_M for 7-methylguanosine. This indicates that Asp40 might have some role in leaving group activation, *via* interaction with the N3 of the 9-deazahypoxanthine ring. It was shown before that the N3 is mechanistically important, since 3-deaza-adenosine is not hydrolysed by the enzyme.[17] However, it is not clear whether the lack of activity with 3-deaza-adenosine is caused by the loss of an essential catalytic interaction, by a global electronic rearrangement of the nucleobase, or by the "base flipping" of the 3-deaza-adenine ring resulting in a catalytically incompetent *syn* conformation, as observed in the *Tv*NH–3-deaza-adenosine crystal structure.

Discussion

The closed-form *T. vivax* IAG-NH: implications for the catalytic mechanism

All previous crystal structures of *Tv*NH showed the active site in the open conformation, with two unstructured flexible loops in the vicinity of the active site.[17,18] Binding of a substrate or a substrate analogue ordered one of these two loops (loop 1), bringing Trp83 into the active site, hence completing an aromatic stacking sandwich involving the purine ring, Trp83 and Trp260.[18] In the work presented here, co-crystallisation of *Tv*NH with the transition-state analogue ImmH has resulted in ordering of the second loop (loop 2), forming the closed active site conformation for the first time with the entire active site visible. Soaking of the same inhibitor in the active site of a pre-existing protein crystal failed to induce the same changes, and leaves the enzyme in a completely open form with both loops largely disordered. The observed large-scale conformational changes associated with loop closure, with a nearly 3° rotation of the two subunits toward each other, are probably prevented by the crystal packing contacts.

Nucleoside hydrolases are believed to reach their tremendous catalytic power (~17.7 kcal/mol)[34] for the hydrolysis of purine and pyrimidine nucleosides using a combination of three strategies: activation of the nucleophile using Asp10 as a general base aided by the Ca^{2+}, steric and electrostatic stabilisation of the oxocarbenium

† Ribose release is known to be the rate-determining step in the hydrolytic direction under steady-state conditions. k_{cat} therefore indicates the rate of ribose release and not the rate of chemistry. k_{cat}/K_M reports on steps up to and including the first irreversible step. Recent transient kinetic data indicate this to be either the *N*-glycosidic bond cleavage step or the base release step.

ion and activation of the leaving nucleobase. The *Tv*NH-ImmH(co) structure, which contains a fully ordered leaving group pocket, now allows us to refine the current model for the catalytic mechanism of group II nucleoside hydrolases.

Ribose binding pocket

All the *Tv*NH crystal structures show the ribose moiety of the nucleoside tightly bound buried away from solvent, with its hydroxyl groups interacting with one or more amino acid residues (see also Table 4). The 2′ and 3′ hydroxyl groups also interact with the Ca^{2+}. Many of the ribose-interacting residues have been shown to be involved both in catalysis and in substrate binding.[35] The multiple enzyme–ribose interactions may be exploited for catalysis in several ways. Incremental binding energy can be utilised to distort the ribose ring in a reactive geometry during transition-state formation (steric catalysis). Additionally, the interactions could partially deprotonate the hydroxyl groups and stabilise the developing positive charge on the oxocarbenium (electrostatic catalysis).[36] Such catalytic interactions are expected to be stronger in the transition-state than in the ground state. However, within the error margins of the crystal structure, only the Asn186-N4′ interaction is significantly shorter in the *Tv*NH–ImmH(co) complex compared to the corresponding Asn186-O4′ interaction in the ground state complexes (3.05 Å *versus* 3.88 Å). Moreover, this change may be artificially increased as a result of the positive charge at the N4′.[27,37] In contrast, the corresponding O4′ remains partially negatively charged, even in the oxocarbenium-ion transition state.[38] This is nicely illustrated by a molecular dynamics study comparing the binding of protonated *p*-aminophenyl-(1*S*)-iminoribitol (pAPIR) to the IU-NH from *C. fasciculata* with the binding of the ground state and transition state of inosine.[39] The calculated Asn168(OD1)-N4′ distance for protonated pAPIR was 2.9 Å, which is in good agreement with the Asn186(OD1)-N4′ distance in our structure. The calculated Asn168(OD1)-O4′ distance on the other hand was 4.4 Å and 3.8 Å for ground state and transition-state inosine, respectively. Although the short Asn186-N4′ interaction might not be fully relevant to the reaction mechanism it could account for the tight binding of ImmH. Hydrogen bonds between charged groups and uncharged groups can be worth ~ 4 kcal/mol,[40] similar to the observed increase in binding energy of ImmH relative to the natural substrates.

Purine binding pocket

Activation of the leaving group by N7 protonation is another recurring catalytic strategy in both non-enzymatic[41] and enzymatic cleavage[42] of *N*-glycosidic bonds in purine nucleosides. Kinetic isotope effect studies have shown that several purine *N*-ribosyltransferases (including the IU-NH from *C. fasciculata*,[20] PNPs,[43] and PRTs[44]) proceed by a mechanism involving pre-equilibrium protonation at N7. Protonation of the nucleoside base by an enzymatic general acid prior to reaching the transition-state facilitates departure of an uncharged leaving nucleobase. In the group I IU-NH from *C. fasciculata*, mutagenesis studies identified a histidine (His241) as the most likely candidate for the role of general acid.[45] This histidine is replaced by a tryptophan (Trp260) in the group II IAG-NH from *T. vivax*. Trp260, together with Trp83, forms a parallel π–π-stacking interaction with the nucleobase. Using experimental approaches and *ab initio* quantum chemical studies, we recently showed that this parallel aromatic stacking interaction between the purine ring of the substrate and Trp260 activates the purine leaving group by raising the pK_a of N7, hence facilitating its protonation.[33] Using the same approach, we subsequently showed that the substrate 5′OH also contributes to the activation of the nucleic base *via* an unusual intra-molecular O5′–HC8 hydrogen bond.[38] Combined together, aromatic stacking with Trp260 and the intramolecular O5′–H–C8 hydrogen bond formation could raise the pK_a of a purine nucleoside sufficiently to promote direct protonation by solvent. The present findings give clear structural support for this mechanism. The completely closed active site of the *Tv*NH–ImmH(co) complex shows only four interaction partners with the nucleobase: Trp260, Trp83, Arg252 and Asp40 (see Figure 4), the latter three seemingly having no prominent role in leaving group activation. The Trp260 side-chain on the other hand approaches the N7 by 0.6 Å in the transition-state structure, corroborating its central role in leaving group activation. The N7 does not interact with an amino acid residue, but is connected to bulk solvent by a network of highly ordered water molecules (Figure 5). This water channel, aided by the polar residues lining it (e.g. Arg252 and Asp255), could act as a proton relay system shuttling protons directly to the high pK_a N7.

A mechanism for loop closure and possible implications for active site communication

The *Tv*NH-ImmH(co) crystal structure provides a clue for a mechanism leading to closure of loop 2 (see Figure 6 and Results for details). This mechanism links the 2′OH group of the substrate/inhibitor *via* a conformational change of Asp14 and Trp242 to loop closure. The actual trigger for this process remains elusive. Conceivably, binding of ImmH, induces the "flipping" of Trp242, which in its turn forces Asp14 into one determined, catalytic conformation. Alternatively, a stronger 2′OH-Asp14 interaction in the ImmH complex causes restraining of Asp14 in one catalytic conformation by itself, with the torsional flip of the Trp242 side-chain filling up the gap left by Asp14 as a second event. The catalytic conformation of Asp14 then allows

interaction with Tyr257, after the latter has moved into the active site with concomitant release of the bridging water molecule. The dislocation of Tyr257 finally frees the space for loop 2 to adopt the closed conformation.

Binding of ImmH to *Tv*NH and the concomitant loop ordering is also accompanied by changes in quaternary structure that suggest a form of inter-subunit active-site communication. In the *Tv*NH-ImmH(co) structure the subunit interface area is significantly increased by more than 40% compared to the unliganded structure (1232 Å^2 compared to 876 Å^2, see Figure 3). This indicates a stabilisation of the dimeric form of the enzyme associated with catalysis. The increase of the subunit interface area is caused by the ordering of loops 1 and 2 upon ImmH binding, with α10 of one subunit interacting with α3 and the loop connecting β2 to α2 of the other subunit. Therefore the dimeric form is probably also required for the proper structuring of loops 1 and 2. These three regions moreover contain active site residues: Trp260 and Arg252 are part of α10, Trp83 is part of α3 and Asp40 is located in the loop connecting β2 to α2. These observations indicate a reciprocal relationship between enzyme activity and its quaternary structure.

A form of active site communication that has been reported for *Tv*NH is its apparent half-the-sites activity that has been observed during substrate turnover.[28] The trimeric calf spleen PNP also displays extreme negative cooperativity, with one-third-the-sites reactivity reported for both inosine hydrolysis and ImmH binding.[21,46] In contrast, the active site titration with PzImmH and the full occupancy of both active sites with ImmH in our crystal structures demonstrate that immucillins bind with full-sites activity in *Tv*NH. Moreover, no significant asymmetry between the subunits that could account for the negative cooperativity can be discerned in the *Tv*NH dimer. The reason for this apparent discrepancy is under investigation.

A role of loop closure in the kinetic mechanism

*Tv*NH follows a complex multi-step mechanism where release of products rather than chemistry forms the rate-limiting step.[28] Previous stopped-flow fluorescence binding experiments showed that both substrate and product ribose binding are two-step processes, consisting of an initial binding step followed by an isomerisation step. For ribose, the kinetics of the isomerisation step indicate that this is the rate-determining step in the hydrolytic direction. A plausible structural explanation for these isomerisation steps is movement of loop 2. Similar roles for active site loop movement in slow, two-step product release have also been described for OMP synthase[8] and the HGXPRT of *Tritrichomonas foetus*.[47] Whether in *Tv*NH loop 2 is actually involved in the slow product release would have to be tested by direct measurement of loop dynamics. However, our steady-state kinetic data on the loop mutants are indicative for such a role. Arg252 is located at the tip of loop 2 and is translocated into the active site to form an interaction with the substrate, upon closure of the loop. When the Arg252 side-chain is deleted we observe a slightly faster release of products from the active site (fivefold higher k_{cat}, see Table 5). An increased k_{cat} (>threefold) was also previously observed for the hydrolysis of inosine by the Tyr257Ala mutant.[18] This tyrosine is a central player in our proposed mechanism for loop closure. These data could indicate a possible involvement of loop 2 dynamics in the rate-limiting conformational changes associated with substrate binding and product release although more direct evidence is certainly required.

The role of loop 2 in chemistry?

Proteins are dynamic molecular machines, and conformational fluctuations on a wide range of time-scales are intimately associated with protein function and may even limit the overall turnover rate.[1,48] Complexes with tight binding transition-state analogues, such as *Tv*NH-ImmH(co), have the effect of "freezing" these motions at some point closely related to the transition state.[24] Thus, the dynamic nature of the transition state is captured and immobilised in the thermodynamic state of the enzyme–transition state complex. The importance of mobile active site loops for catalysis has been rationalised on the basis that they permit both the rate of substrate binding and the amount of binding energy between enzyme and substrate to be maximised.[49] In addition to providing binding energy (by providing catalytically essential residues), loops may also play a "negative catalysis" role by protecting reactive intermediates from solvolysis.[50] Mobile active site loops that sequester bound substrate or inhibitor from solvent are a common feature of *N*-ribosyltransferases. It has been proposed for both PNPs[4] and PRTs[6] that exclusion of bulk solvent during catalysis reduces the extent of hydrolysis of the (labile) intermediates. This negative catalytic function is clearly not applicable for the hydrolytic *Tv*NH reaction.

Mutagenesis of the loop 2 residue Arg252 has only a small effect on the steady-state kinetics of *Tv*NH with guanosine, adenosine, 7-methylguanosine and purine riboside. Similar small effects on the steady-state kinetics were previously observed during an alanine scan of loop 2 using inosine as substrate.[18] Thus, specific interactions between substrate and the side-chains of loop 2 do not appear to be essential for catalysis. A first formal explanation for these mutagenesis results may be that the loop has a non-catalytic role or is possibly a vestigial structure that has lost its function. Alternatively, the role of the loop may be to alter a more global property, such as the dielectric or the shape of the active site. Single residue mutagenesis may not be sufficient to significantly perturb such global properties.

Materials and Methods

Expression and purification

Expression and purification of the wild-type and mutant *T. vivax* IAG-NHs were performed as described.[17] *Escherichia coli* (WK6) containing the *iagnh* ORF cloned in the pQE-30 expression vector (Qiagen) was used for recombinant protein production. The presence of an N-terminal His_6-tag permitted purification in two chromatographic steps, consisting of a Ni-NTA affinity chromatography step (Qiagen) and gel filtration on a Superdex-200 column (Amersham Bioscience). The concentration of pure protein (expressed per monomer) was determined spectrophotometrically using an ε_{280} of 47,752 $M^{-1}cm^{-1}$. Typically, 80 mg of purified protein was obtained from a 1 l fermentation. SDS-polyacrylamide gel electrophoresis was used to confirm enzyme purity.

Kinetic analysis of substrates

Initial rate kinetic measurements were carried out at 35 °C in 20 mM Hepes buffer (pH 7.0), containing 150 mM NaCl and 1 mM $CaCl_2$. Product formation was determined spectrophotometrically using the difference in absorption between the nucleoside and the purine base.[18] The $\Delta\varepsilon$ values ($mM^{-1}\,cm^{-1}$) used were: guanosine, −4.0 at 260 nm or 0.5 at 300 nm; 7-methylguanosine, −4.4 at 258 nm; adenosine, −1.4 at 276 nm; purine riboside, 1.45 at 275 nm. The kinetic properties for cytidine were determined with the reducing sugar assay as described.[18]

Inhibition studies

Inhibitor dissociation constants were determined with inosine as a substrate in 50 mM phosphate (pH 7.5) at 25 °C. A coupled assay using xanthine oxidase was used to monitor inosine hydrolysis.[51] The reaction product hypoxanthine is oxidised to uric acid, which can be monitored spectrophotometrically at 293 nm ($\Delta\varepsilon$ uric acid at 293 nm = 12.9 $mM^{-1}\,cm^{-1}$). Reactions were started by adding the wild-type or mutant NH to the reaction mixture containing 500 μM inosine, 120 mU xanthine oxidase/ml and a variable concentration of inhibitor. The Michaelis constants for inosine hydrolysis were determined under the same conditions. The inhibitor set was initially assayed at 50 μM to identify tight binders. The binding properties of the three tight binders that were thus identified (PzImmH, ImmH and ImmA) were then analysed further. Time-courses that displayed slow-onset behaviour were fitted to the equation:[52]

$$P = v_s t + (v_0 - v_s)(1 - e^{-kt})/k \quad (1)$$

where P is product concentration, v_s and v_0 are the steady-state and initial reaction rates, respectively, k is the apparent first-order rate constant for attaining the steady-state, and t is time. K_i and K_i^* were obtained, respectively, by plotting v_o or v_s *versus* inhibitor concentration and performing non-linear curve fitting (Origin v.7) to the equations:

$$v_0 = VA/[K_M(1 + I/K_i) + A] \quad (2)$$

$$v_s = VA/[K_M(1 + I/K_i^*) + A] \quad (3)$$

where A is the substrate concentration, V is the maximal velocity and K_M is the Michaelis constant. For ImmH and ImmA, which did not display slow-onset inhibition over a 180 min period, K_i was estimated from the plots of v_0 *versus* I as above.

Active site titrations were carried out by pre-incubating *Tv*NH (6 μM monomer) with different concentrations of inhibitor (0–1.4 equivalents inhibitor/*Tv*NH monomer) in 50 mM phosphate (pH 7.5) at 4 °C for 16 h. Samples were then rapidly diluted 40-fold into the same buffer, followed by a 25-fold dilution into the xanthine oxidase assay mix as described above for a total dilution of 1000-fold. Rebinding of inhibitor to *Tv*NH was prevented with high concentrations of substrate (500 μM ≈ 200 × K_m; final inhibitor concentration at ≈ K_i; k_{on} for substrate and inhibitor are known to be approximately equal from stopped-flow measurements). Time-courses were fitted to the equation:

$$P = v_s t + (v_r - v_s)(1 - e^{-kt})/k \quad (4)$$

where v_r is the initial velocity ($v_r < v_s$). For PzImmH, the binding stoichiometry was determined from a plot of v_r *versus* [I/(*Tv*NH monomer] and then extrapolating the linear decrease in v_r to the x-intercept. The value of k was also approximately constant above one equivalent inhibitor/(*Tv*NH monomer) and the saturated value of k was therefore equated to k_6 (see Scheme 1). k_5 was calculated using the equation:

$$k_5 = k_6(K_i/K_i^* - 1) \quad (5)$$

Crystallisation, data collection and processing

X-ray diffraction datasets were collected for two different *Tv*NH-ImmH complexes: one of a co-crystallised complex (*Tv*NH-ImmH(co)), and one of a crystal soaked in the inhibitor solution (*Tv*NH-ImmH(soak)). For co-crystallisation, a solution of 8 mg/ml wild-type *Tv*NH in 20 mM Hepes (pH 7.0), 150 mM NaCl, 1 mM $CaCl_2$ was pre-incubated with a 1:2 molar excess of inhibitor for 1 h at 4 °C. Crystals of both complexed and the unliganded *Tv*NH protein were grown using the hanging-drop, vapour-diffusion method. Equal volumes of protein solution (8 mg/ml) and precipitant containing 1.6 M ammonium sulphate in 100 mM Tris buffer (pH 8.5) were mixed and equilibrated at 20 °C. The crystals of the complexed protein were transferred to a cryo-solution containing 1.8 M ammonium sulphate, 100 mM Tris (pH 8.5) and 30% (v/v) glycerol and X-ray diffraction data were collected to a resolution of 2.2 Å at 100 K on beamline X11 (EMBL, DESY, Hamburg) using an X-ray wavelength of 0.8131 Å. The crystals of the "unliganded" protein were soaked in a cryo-solution containing 40% (w/v) PEG 6000 in 100 mM Hepes buffer (pH 7.0) and 1.2 mM ImmH. After several hours crystals were transferred to the cryo-stream (100 K) and data were collected to a resolution of 2.0 Å on beamline BW7A (EMBL, DESY, Hamburg) using an X-ray wavelength of 0.9322 Å.

The diffraction data were integrated, scaled and merged with the HKL package.[53] Intensities were converted to structure factors using TRUNCATE.[54] Relevant statistics for both datasets are summarised in Table 2.

Structure determination and refinement

The co-ordinates of one monomer of the wild-type *T. vivax* IAG-NH (pdb 1HOZ), with all the ligands and flexible parts removed, were used as a search model to

solve the structure of the co-crystallised *Tv*NH–ImmH complex by molecular replacement using Phaser.[55] After a first round of simulated annealing refinement[56] in CNS, several cycles of positional and *B*-factor refinement using CNS[57] were alternated with manual rebuilding in sigmaA-weighted ($2F_o-F_c$, ϕ_c) and (F_o-F_c, ϕ_c) electron density maps using TURBO-FRODO.[58] The ($2F_o-F_c$, ϕ_c) and (F_o-F_c, ϕ_c) electron density maps in both active sites in the asymmetric unit showed unambiguous electron density for ImmH after the initial rounds of refinement and the entire protein backbone could be traced. After refinement an *R*-factor of 16.74% was obtained (free *R*-factor of 22.61%).

The crystal structure of the *Tv*NH soaked with ImmH is isomorphous to the unliganded *Tv*NH structure (PDB 1HOZ). Therefore, refinement was started from the latter model (without solvent and ligands and with all flexible parts removed), taking care to use the same set of reflections for cross-validation. The refinement procedure used was the same as stated above. The ($2F_o-F_c$, ϕ_c) and (F_o-F_c, ϕ_c) maps in both active sites in the asymmetric unit showed unambiguous electron density for ImmH. Amino acid residues 245 to 257 in the A subunit and amino acid residues 245 to 255 in the B subunit were excluded from the model, due to very weak electron density in this region. The final model provided an *R*-factor of 17.81% (free *R*-factor 22.52%).

During the refinement, the quality of the models was monitored with PROCHECK.[59]

Protein Data Bank accession codes

The coordinates and structure factors have been deposited with the RCSB Protein Data Bank, accession code 2FF1 for *Tv*NH–ImmH(soak) and 2FF2 for *Tv*NH–ImmH(co).

Acknowledgements

The authors thank V.L. Schramm, Albert Einstein College of Medicine, Bronx, New York, for providing the inhibitors and laboratory access for the values in Table 1. Inhibitors were synthesized by G.B. Evans and P.C. Tyler, Carbohydrate Chemistry Team, Industrial Research Ltd, Lower Hutt, New Zealand. The authors acknowledge the EMBL for use of beamlines BW7-A and X11 (DESY, Hamburg, Germany). Supported by research grants of the IWT-Vlaanderen and the Fund for Scientific Research-Flanders (FWO-Vlaanderen). W.V. thanks the FWO-Vlaanderen for a postdoctoral grant.

References

1. Eisenmesser, E. Z., Millet, O., Labeikovsky, W., Korzhnev, D. M., Wolf-Watz, M., Bosco, D. A. *et al.* (2005). Intrinsic dynamics of an enzyme underlies catalysis. *Nature*, **438**, 36–37.
2. McElheny, D., Schnell, J. R., Lansing, J. C., Dyson, H. J. & Wright, P. E. (2005). Defining the role of active-site loop fluctuations in dihydrofolate reductase catalysis. *Proc. Natl Acad. Sci. USA*, **102**, 5032–5037.
3. Desamero, R., Rozovsky, S., Zhadin, N., McDermott, A. & Callender, R. (2003). Active site loop motion in triosephosphate isomerase: T-jump relaxation spectroscopy of thermal activation. *Biochemistry*, **42**, 2941–2951.
4. Fedorov, A., Shi, W., Kicska, G., Fedorov, E., Tyler, P. C., Furneaux, R. H. *et al.* (2001). Transition state structure of purine nucleoside phosphorylase and principles of atomic motion. *Biochemistry*, **40**, 853–860.
5. Koellner, G., Bzowska, A., Wielgus-Kutrowska, B., Luic, M., Steiner, T., Saenger, W. & Stepinski, J. (2002). Open and closed conformation of the *E. coli* purine nucleoside phosphorylase active center and implications for the catalytic mechanism. *J. Mol. Biol.* **315**, 351–371.
6. Shi, W., Li, C. M., Tyler, P. C., Furneaux, R. H., Grubmeyer, C., Schramm, V. L. & Almo, S. C. (1999). The 2.0 Å structure of human hypoxanthine-guanine phosphoribosyltransferase in complex with a transition-state analog inhibitor. *Nature Struct. Biol.* **6**, 588–593.
7. Munagala, N., Basus, V. J. & Wang, C. C. (2001). Role of the flexible loop of hypoxanthine-guanine-xanthine phosphoribosyltransferase from *Tritrichomonas foetus* in enzyme catalysis. *Biochemistry*, **40**, 4303–4311.
8. Wang, G. P., Cahill, S. M., Liu, X., Girvin, M. E. & Grubmeyer, C. (1999). Motional dynamics of the catalytic loop in OMP synthase. *Biochemistry*, **38**, 284–295.
9. Degano, M., Almo, S. C., Sacchettini, J. C. & Schramm, V. L. (1998). Trypanosomal nucleoside hydrolase. A novel mechanism from the structure with a transition-state inhibitor. *Biochemistry*, **37**, 6277–6285.
10. Versées, W. & Steyaert, J. (2003). Catalysis by nucleoside hydrolases. *Curr. Opin. Struct. Biol.* **13**, 731–738.
11. Hammond, D. J. & Gutteridge, W. E. (1984). Purine and pyrimidine metabolism in the *Trypanosomatidae*. *Mol. Biochem. Parasitol.* **13**, 243–261.
12. Berens, R. L., Krug, E. D. & Marr, J. J. (1995). Purine and pyrimidine metabolism. In *Biochemistry and Molecular Biology of Parasites* (Marr, J. J. & Müller, M., eds), pp. 89–117, Academic Press, London.
13. Bennett, E. M., Anand, R., Allan, P. W., Hassan, A. E., Hong, J. S., Levasseur, D. N. *et al.* (2003). Designer gene therapy using an *Escherichia coli* purine nucleoside phosphorylase/prodrug system. *Chem. Biol.* **10**, 1173–1181.
14. Ranquin, A., Versées, W., Wolfgang, M., Steyaert, J. & Van Gelder, P. (2005). Therapautic nanoreactors: combining chemistry and biology in a novel triblock copolymer drug delivery system. *Nano Letters*, **5**, 2220–2224.
15. Giabbai, B. & Degano, M. (2004). Crystal structure to 1.7 Å of the *Escherichia coli* pyrimidine nucleoside hydrolase YeiK, a novel candidate for cancer gene therapy. *Structure*, **12**, 739–749.
16. Degano, M., Gopaul, D. N., Scapin, G., Schramm, V. L. & Sacchettini, J. C. (1996). Three-dimensional structure of the inosine-uridine nucleoside *N*-ribohydrolase from *Crithidia fasciculata*. *Biochemistry*, **35**, 5971–5980.
17. Versées, W., Decanniere, K., Pellé, R., Depoorter, J., Brosens, E., Parkin, D. W. & Steyaert, J. (2001). Structure and function of a novel purine specific nucleoside hydrolase from *Trypanosoma vivax*. *J. Mol. Biol.* **307**, 1363–1379.
18. Versées, W., Decanniere, K., Van Holsbeke, E., Devroede, N. & Steyaert, J. (2002). Enzyme-substrate

interactions in the purine-specific nucleoside hydrolase from *Trypanosoma vivax*. *J. Biol. Chem.* **277**, 15938–15946.
19. Schramm, V. L. (2003). Enzymatic transition state poise and transition state analogues. *Accts Chem. Res.* **36**, 588–596.
20. Horenstein, B. A., Parkin, D. W., Estupiñán, B. & Schramm, V. L. (1991). Transition-state analysis of nucleoside hydrolase from *Crithidia fasciculata*. *Biochemistry*, **30**, 10788–10795.
21. Miles, R. W., Tyler, P. C., Furneaux, R. H., Bagdassarian, C. K. & Schramm, V. L. (1998). One-third-the-sites transition-state inhibitors for purine nucleoside phosphorylase. *Biochemistry*, **37**, 8615–8621.
22. Kicska, G., Long, L., Horig, H., Fairchild, C., Tyler, P. C., Furneaux, R. H. *et al*. (2001). Immucillin H, a powerful transition-state analog inhibitor of purine nucleoside phosphorylase, selectively inhibits human T lymphocytes. *Proc. Natl Acad. Sci. USA*, **98**, 4593–4598.
23. Miles, R. W., Tyler, P. C., Evans, G. B., Furneaux, R. H., Parkin, D. W. & Schramm, V. L. (1999). Iminoribitol transition state analogue inhibitors of protozoan nucleoside hydrolases. *Biochemistry*, **38**, 13147–13154.
24. Schramm, V. L. (2005). Enzymatic transition states: thermodynamics, dynamics and analogue design. *Arch. Biochem. Biophys.* **433**, 13–26.
25. Lewandowicz, A., Shi, W., Evans, G. B., Tyler, P. C., Furneaux, R. H., Basso, L. A. *et al*. (2003). Over-the-barrier transition state analogues and crystal structure with *Mycobacterium tuberculosis* purine nucleoside phosphorylase. *Biochemistry*, **42**, 6057–6066.
26. Evans, G. B., Furneaux, R. H., Gainsford, G. J., Hanson, J. C., Kicska, G., Sauve, A. A. *et al*. (2003). 8-Aza-immucillins as transition-state analogue inhibitors of purine nucleoside phosphorylase and nucleoside hydrolase. *J. Med. Chem.* **46**, 155–160.
27. Parkin, D. W. & Schramm, V. L. (1995). Binding modes for substrate and a proposed transition-state analogue of protozoan nucleoside hydrolase. *Biochemistry*, **34**, 13961–13966.
28. Vandemeulebroucke, A., Versées, W., De Vos, S., Van Holsbeke, E. & Steyaert, J. (2003). Pre-steady state analysis of the nucleoside hydrolase of *Trypanosoma vivax*. Evidence for half-of-the-sites reactivity and rate-limiting product release. *Biochemistry*, **42**, 12902–12908.
29. Altona, C. & Sundaralingam, M. (1972). Conformational analysis of the sugar ring in nucleosides and nucleotides. *J. Am. Chem. Soc.* **94**, 8212.
30. Mazumder-Shivakumar, D. & Bruice, T. C. (2005). Computational study of IAG-nucleoside hydrolase: determination of the preferred ground state conformation and the role of active site residues. *Biochemistry*, **44**, 7805–7817.
31. Sauve, A. A., Cahill, S. M., Zech, S. G., Basso, L. A., Lewandowicz, A., Santos, D. S. *et al*. (2003). Ionic states of substrates and transition state analogues at the catalytic sites of *N*-ribosyltransferases. *Biochemistry*, **42**, 5694–5705.
32. Kulikowska, E., Bzowska, A., Wierzchowski, J. & Shugar, D. (1986). Properties of two unusual, and fluorescent, substrates of purine-nucleoside phosphorylase: 7-methylguanosine and 7-methylinosine. *Biochim. Biophys. Acta*, **874**, 355–363.
33. Versées, W., Loverix, S., Vandemeulebroucke, A., Geerlings, P. & Steyaert, J. (2004). Leaving group activation by aromatic stacking: an alternative to general acid catalysis. *J. Mol. Biol.* **338**, 1–6.
34. Parkin, D. W., Limberg, G., Tyler, P. C., Furneaux, R. H., Chen, X.-Y. & Schramm, V. L. (1997). Isozyme-specific transition state inhibitors for the trypanosomal nucleoside hydrolases. *Biochemistry*, **36**, 3528–3534.
35. Versées, W. (2002). Structure and function of the inosine-adenosine-guanosine preferring nucleoside hydrolase from *Trypanosoma vivax*. PhD thesis, Vrije Universiteit Brussel.
36. Singh, V., Lee, J. E., Nunez, S., Howell, P. L. & Schramm, V. L. (2005). Transition state structure of 5′-methylthioadenosine/*S*-adenosylhomocysteine nucleosidase from *Escherichia coli* and its similarity to transition state analogues. *Biochemistry*, **44**, 11647–11659.
37. Mazumder, D., Kahn, K. & Bruice, T. C. (2002). Computer simulations of Trypanosomal nucleoside hydrolase: determination of the protonation state of the bound transition-state analogue. *J. Am. Chem. Soc.* **124**, 8825–8833.
38. Loverix, S., Geerlings, P., McNaughton, M., Augustyns, K., Vandemeulebroucke, A., Steyaert, J. & Versées, W. (2005). Substrate-assisted leaving group activation in enzyme-catalyzed N-glycosidic bond cleavage. *J. Biol. Chem.* **280**, 14799–14802.
39. Mazumder, D. & Bruice, T. C. (2002). Exploring nucleoside hydrolase catalysis *in silico*: molecular dynamics study of enzyme-bound substrate and transition state. *J. Am. Chem. Soc.* **124**, 14591–14600.
40. Fersht, A. R. (1985). *Enzyme Structure and Mechanism*, W. H. Freeman and Company, New York.
41. Zoltewicz, J. A., Clark, D. F., Sharpless, T. W. & Grahe, G. (1970). Kinetics and mechanism of the acid-catalyzed hydrolysis of some purine nucleosides. *J. Am. Chem. Soc.* **92**, 1741–1750.
42. Schramm, V. L. (1998). Enzymatic transition states and transition state analog design. *Annu. Rev. Biochem.* **67**, 693–720.
43. Kline, P. C. & Schramm, V. L. (1993). Purine nucleoside phosphorylase. Catalytic mechanism and transition-state analysis of the arsenolysis reaction. *Biochemistry*, **32**, 13212–13219.
44. Xu, Y. & Grubmeyer, C. (1998). Catalysis in human hypoxanthine-guanine phosphoribosyltransferase: Asp137 acts as a general acid/base. *Biochemistry*, **37**, 4114–4124.
45. Gopaul, D. N., Meyer, S. L., Degano, M., Sacchettini, J. C. & Schramm, V. L. (1996). Inosine-uridine nucleoside hydrolase from *Crithidia fasciculata*. Genetic characterization, crystallization, and identification of histidine 241 as a catalytic site residue. *Biochemistry*, **35**, 5963–5970.
46. Kline, P. C. & Schramm, V. L. (1995). Pre-steady-state transition-state analysis of the hydrolytic reaction catalyzed by purine nucleoside phosphorylase. *Biochemistry*, **34**, 1153–1162.
47. Munagala, N., Basus, V. J. & Wang, C. C. (2001). Role of the flexible loop of hypoxanthine-guanine-xanthine phosphoribosyltransferase from *Tritrichomonas foetus* in enzyme catalysis. *Biochemistry*, **40**, 4303–4311.
48. Benkovic, S. J. & Hammes-Schiffer, S. (2003). A perspective on enzyme catalysis. *Science*, **301**, 1196–1202.
49. Wolfenden, R. (1999). Conformational aspects of inhibitor design: enzyme–substrate interactions in the transition state. *Bioorg. Med. Chem.* **7**, 647–652.
50. Knowles, J. R. (1991). Enzyme catalysis: not different, just better. *Nature*, **350**, 121–124.
51. Lewandowicz, A., Ringia, E. A., Ting, L. M., Kim, K., Tyler, P. C., Evans, G. B. *et al*. (2005). Energetic

mapping of transition state analogue interactions with human and *Plasmodium falciparum* purine nucleoside phosphorylases. *J. Biol. Chem.* **280**, 30320–30328.
52. Morrison, J. F. & Walsh, C. T. (1988). The behavior and significance of slow-binding enzyme inhibitors. *Advan. Enzymol. Relat. Areas Mol. Biol.* **61**, 201–301.
53. Otwinowski, Z. & Minor, W. (1997). Processing of X-ray diffraction data collected in oscillation mode. In *Methods in Enzymology Macromolecular Crystallography Part A* (Carter, C. W. & Sweet, R. M., eds), vol. 276, pp. 307–326, Academic Press, New York.
54. French, S. & Wilson, K. (1978). On the treatment of negative intensity observations. *Acta Crystallog. sect. A*, **34**, 517–525.
55. McCoy, A. J., Grosse-Kunstleve, R. W., Storoni, L. C. & Read, R. J. (2005). Likelihood-enhanced fast translation functions. *Acta Crystallog. sect. D*, **61**, 458–464.
56. Brünger, A. T., Krukowski, A. & Erickson, J. W. (1990). Slow-cooling protocols for crystallographic refinement by simulated annealing. *Acta Crystallog. sect. A*, **46**, 585–593.
57. Brünger, A. T., Adams, P. D., Clore, G. M., DeLano, W. L., Gros, P., Grosse-Kunstleve, R. W. *et al.* (1998). Crystallography and NMR system (CNS): a new software system for macromolecular structure determination. *Acta Crystallog. sect. D*, **54**, 905–921.
58. Roussel, A., Fontecilla-Camps, J. C. & Cambillau, C. (1990). TURBO-FRODO: a new program for protein crystallography and modelling. *XV IUCr Congress Abstracts, Bordeaux, France*, 66–67.
59. Laskowski, R. A., MacArthur, M. W., Moss, D. S. & Thornton, J. M. (1993). PROCHECK–a progam to check the stereochemical quality of proteins. *J. Appl. Crystallog.* **26**, 283–291.
60. DeLano, W. L. (2002). *The PyMOL Molecular Graphics System*, DeLano Scientific, San Carlos, CA, USA.
61. Kraulis, P. J. (1991). MOLSCRIPT: a program to produce both detailed and schematic plots of protein structures. *J. Appl. Crystallog.* **24**, 946–950.
62. Luzzati, V. (1952). Traitement statistique des erreurs dans la determination des structures cristallines. *Acta Crystallog.* **5**, 802–810.
63. Vaguine, A. A., Richelle, J. & Wodak, S. J. (1999). SFCHECK: a unified set of procedures for evaluating the quality of macromolecular structure-factor data and their agreement with the atomic model. *Acta Crystallog. sect. D*, **55**, 191–205.

Edited by R. Huber

(Received 22 December 2005; received in revised form 8 March 2006; accepted 14 March 2006)